Archives of Biochemistry and Biophysics 771 (2025) 110523

Contents lists available at ScienceDirect

Archives of Biochemistry and Biophysics

journal homepage: www.elsevier.com/locate/yabbi

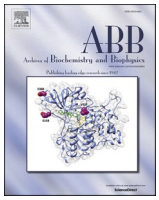

Instability and resilience at the lipid membrane interface under ultrasound: composition matters

Alexandre Blanco-González [a,b,c], Ángel Piñeiro [b,*], Rebeca García-Fandiño [a,**]

[a] Departamento de Química Orgánica, Centro Singular de Investigación en Química Biolóxica e Materiais Moleculares (CiQUS), Universidade de Santiago de Compostela, Campus Vida s/n, E-15782, Santiago de Compostela, Spain
[b] Departamento de Física Aplicada, Facultade de Física, Universidade de Santiago de Compostela, E-15782, Santiago de Compostela, Spain
[c] MD.USE Innovations S.L., Edificio Emprendia, 15782, Santiago de Compostela, Spain

ARTICLE INFO

Keywords:
Molecular dynamics
Lipid membranes
Ultrasounds
Frequency
Amplitude

ABSTRACT

Lipid membranes play a crucial role in cellular function, acting not only as structural barriers but also facilitating key biological processes such as selective permeability, signaling, and mechanical stability. The composition of these membranes varies significantly across different cell types, species, and disease states, influencing their mechanical properties and susceptibility to disruption. This variability presents an opportunity to selectively target pathological cells based on their unique lipid profiles, potentially allowing for the precise disruption of diseased cells while sparing healthy ones. Additionally, focused ultrasound (FUS) has emerged as a promising tool for modulating membrane integrity, with applications in targeted drug delivery and cancer therapy. However, the precise interactions between FUS waves and different lipid compositions remain insufficiently understood. This study systematically investigates the effects of varying ultrasound frequencies (5–50 MHz) and overpressures (5–50 bar) on the mechanical responses of four distinct lipid bilayers—POPC, POPE, POPG, and POPS—using molecular dynamics simulations. These lipids are commonly found in mammalian, bacterial, and cancerous cell membranes. Key structural parameters, including area per lipid, curvature, thickness, and lipid tail order, were analyzed to determine how different ultrasound conditions affect membrane integrity. The results reveal that lipid composition critically determines membrane vulnerability to mechanical perturbations. For instance, POPC membranes are more prone to deformation under certain ultrasound conditions, while POPG and POPS exhibit abrupt transitions to instability at extreme pressures and frequencies. These findings offer valuable insights into the selective tuning of ultrasound parameters for therapeutic applications and highlight the critical role of membrane composition in determining mechanical responses to ultrasound-induced stress.

1. Introduction

Lipid membranes are more than mere structural components; they are dynamic entities that play a fundamental role in biological cells. These bilayered structures not only encapsulate cellular and organelle environments but also serve as pivotal platforms for a myriad of life processes. Their roles extend from facilitating selective permeability to external substances [1], thus maintaining the cell's internal milieu, to providing a fluid film for protein interaction and signaling cascades [2,3]. Lipid membranes are also key in cellular mechanical processes including adhesion, shape, and motility [4]. The versatility of lipid membranes arises from their diverse lipid composition, which can rapidly remodel in response to cellular demands or environmental stimuli, hence playing a decisive role in the adaptive capacity of life. The integrity of biological membranes is critical for cellular survival and function. Disruptions in membrane structure can lead to a sequence of cellular malfunctions, often culminating in disease [5]. Thus, understanding the complex nature of lipid membranes [6] is not only fundamental to the comprehension of cell biology but also key for theranostic purposes.

The lipid composition of cellular membranes is not a static attribute but a dynamic one, rich with biological implications. This variability arises from a confluence of factors, such as phylogenetic differences among species [7], which dictate unique lipidomic signatures that can

Abbreviations: US, Ultrasounds; HIFU, High Intensity Focused Ultrasounds; CG, Coarse Grained; APL, Area Per Lipid.

* Corresponding author.
** Corresponding author.
E-mail addresses: Angel.Pineiro@usc.es (Á. Piñeiro), rebeca.garcia.fandino@usc.es (R. García-Fandiño).

https://doi.org/10.1016/j.abb.2025.110523
Received 26 November 2024; Received in revised form 31 March 2025; Accepted 25 June 2025
Available online 26 June 2025

be thought of as a cellular fingerprint. Within an organism, cellular differentiation processes further diversify lipid profiles, tailoring membranes to the specific needs of each cell type [8]. For instance, mammalian cells typically have a higher proportion of phosphatidylcholine (PC), cholesterol and sphingolipids compared to bacterial cells, which are characterized by a higher content of phosphatidylethanolamine (PE) and unique anionic lipids like phosphatidylglycerol (PG), as well as cardiolipin [9]. This fundamental difference in lipid composition impacts membrane fluidity, permeability, and the functional roles membranes play within these organisms.

The recent explosion of lipidomics has unveiled unique lipid profiles in conditions such as cancer [10], viral and bacterial infections [11], and even in senescent cells associated with aging [12], opening avenues for the use of the cell membrane as a biomarker and therapeutic target. Noteworthy alterations include the presence of phosphatidylglycerol (PG), an anionic lipid in bacterial membranes, or the loss of asymmetry between leaflets in cancer cell membranes, exposing phosphatidylserine (PS), an anionic lipid, to the outer monolayer. Additionally, aging is associated with a decrease in phosphatidylcholine (PC) or phosphatidylethanolamine (PE) levels. These changes highlight the critical role of lipid membranes in health and disease, underscoring the potential of targeting membrane lipids for therapeutic intervention.

Given that lipid composition largely determines the physicochemical and mechanical properties of biological membranes [13,14], various tactics can be employed to selectively destroy certain cells over others. Among the strategies developed by nature is the use of endogenous therapeutic peptides (ETPs) [15], which are key components of the innate immune system across all living organisms. ETPs can recognize foreign lipid patterns, disrupting membranes through various mechanisms [16], while leaving healthy membranes unaffected.

Cellular membranes can also be disrupted through alternative methods, such as mechanical perturbations. In recent years, there has been growing interest in focused ultrasound techniques (FUS), including High-Intensity Focused Ultrasound (HIFU) [17] and histotripsy [18]. Both methods use transducers to concentrate mechanical waves in a millimeter-sized area, penetrating the skin and underlying tissue without invasive surgery. These techniques are promising alternatives to conventional surgical interventions, but the direct impact of focused sound waves on cellular membranes at the molecular level is largely unknown. Proposing new therapies based on mechanical perturbations requires identifying significant differences between the membranes of healthy and diseased cells, in their ability to transmit a mechanical wave or to maintain their integrity under pressure changes. Given the extensive evidence correlating lipid composition with various diseases, it makes sense to investigate potential mechanical vulnerabilities based on specific lipidomic profiles to exploit them for therapeutic purposes [19].

Recent advances in biomedical research have also demonstrated the potential of combining FUS with drug delivery systems to enhance therapeutic efficacy. FUS can temporarily permeabilize cell membranes, a process known as sonoporation, which facilitates the uptake of drugs and other therapeutic agents into targeted cells. This technique, especially when combined with drug-loaded microbubbles or nanoparticles, has shown promise in increasing local drug concentration at disease sites like tumors while minimizing systemic side effects [20,21]. For instance, FUS has been used to enhance drug delivery across the blood-brain barrier, addressing a significant challenge in treating brain tumors and neurological disorders. Additionally, FUS can trigger localized drug release from carriers such as liposomes, concentrating the therapeutic effect at the target site.

While microbubble-assisted sonoporation is the most widely studied mechanism in ultrasound-mediated drug delivery, recent studies have demonstrated that ultrasound alone, particularly at high intensities and specific pulsing regimes, can directly influence lipid bilayer integrity even in the absence of cavitation nuclei. These direct interactions include increased membrane fluidity, transient permeability, and structural deformation, which have been observed in both experimental and computational studies [22–25]. Notably, these effects depend strongly on ultrasound frequency, pressure, and lipid composition, suggesting that targeted mechanical perturbations could be exploited to selectively disrupt specific lipid environments. Understanding these fundamental interactions is critical for optimizing ultrasound-based therapeutic strategies beyond conventional sonoporation.

Molecular dynamics (MD) simulations have emerged as powerful tools to understand these complexities. MD allows for the detailed exploration of the behavior of lipid membranes under various conditions, offering insights into the dynamic-structural responses to mechanical perturbations[26–33]. In a previous study, we used MD simulations to investigate the effects of focused ultrasound mechanotherapy on lipid bilayers [34]. We examined ten distinct lipid compositions, exposing them to an ultrasound wave of 12 MHz frequency and a 35 bar overpressure. Our results indicated that the dynamic-structural response of membrane models to mechanical perturbations caused by sound waves strongly depends on the lipid composition, with properties such as area per lipid (APL), bilayer curvature, tail tilt, and membrane thickness being significantly influenced by mechanical stress. Specifically, ten different membrane compositions were systematically investigated, revealing that the presence of lipids such as 1-palmitoyl-2-oleoyl-sn-glycero-3-phosphocholine (POPC), 1-palmitoyl-2-oleoyl-sn-glycero-3-phosphoethanolamine (POPE), 1-palmitoyl-2-oleoyl-sn-glycero-3-phosphoglycerol (POPG), and 1-palmitoyl-2-oleoyl-sn-glycero-3-phosphoserine (POPS) significantly influences the membranes' sensitivity to US waves. Through these simulations, the impact of mechanical stress on critical properties such as area per lipid, bilayer curvature, tail tilt, and membrane thickness were assessed. The analyses demonstrated that different lipid compositions exhibit varied sensitivities to US-induced perturbations, suggesting the potential for designing lipid membranes with specific responses to predetermined mechanical forces. This understanding paves the way for the rational design of new therapies targeting diseases characterized by distinct lipid profiles.

In the present work, we aim to expand upon these findings by exploring a broader range of frequencies and pressures to determine their influence on the selectivity of mechanical perturbations. To comprehensively explore the parameter space of US wave characteristics, both the frequency and amplitude of the oscillator were systematically varied. Frequencies ranged from 5 to 50 MHz in increments of 5 MHz, while amplitudes spanned from 5 to 50 bar, also in 5 bar increments. This systematic variation is crucial for understanding the mechanistic underpinnings of ultrasound-membrane interactions and for optimizing the conditions under which specific lipid compositions are more susceptible to mechanical disruption. Homogenous lipid bilayers of POPC, POPE, POPG, and POPS, which are representative of typical cellular membranes, will be characterized. This selection is justified by their prevalence in both healthy and diseased states. POPC is the most common lipid in mammalian cell membranes, POPE and POPG are abundant in bacterial membranes, and POPS is often found in cancerous cells. By varying the mechanical parameters, we seek to determine how different frequencies and pressures influence the mechanical response of these lipid bilayers.

2. Methods

The FUS wave was modeled by modifying the implementation of the Berendsen barostat [35] in the GROMACS package, following a previously established protocol [34]. This modification allows for the application of a sinusoidal pressure wave of controlled amplitude and frequency along the membrane's normal axis (Z-axis). In our previous work, lipid bilayers of various compositions were subjected to pressure oscillations at a fixed amplitude of 35 bar and frequency of 12 MHz, using both coarse-grained (CG) and atomic resolution models. Detailed analysis were performed to assess the response of different structural and dynamic descriptors to this pressure perturbation.

The present work expands upon this approach by systematically

varying both the frequency and amplitude of the FUS wave across four different membrane models. The membrane models consisted of pure bilayers of 1-palmitoyl-2-oleoyl-sn-glycero-3-phosphocholine (POPC), 1-palmitoyl-2-oleoyl-sn-glycero-3-phosphoethanolamine (POPE), 1-palmitoyl-2-oleoyl-sn-glycero-3-phosphoglycerol (POPG), and 1-palmitoyl-2-oleoyl-sn-glycero-3-phosphoserine (POPS), each containing a total of 500 lipids. These specific lipids were chosen to represent a diverse range of headgroups and to investigate how these differences might influence the membrane's response to FUS waves. The membranes were parameterized using the Martini 3.0 force field [36,37]. Each bilayer was solvated using a ratio of 50 water molecules per lipid, ensuring adequate hydration for proper membrane behavior. In cases where the lipids carried a net charge (POPG and POPS), Na+ ions were added to achieve charge neutrality. All membrane systems were constructed using the CHARMM-GUI tool[38–41].

To comprehensively explore the parameter space of FUS wave characteristics, both the frequency and amplitude of the oscillator were systematically varied. Frequencies ranged from 5 to 50 MHz in increments of 5 MHz, while amplitudes spanned from 5 to 50 bar, also in 5 bar increments. This resulted in a total of 100 distinct simulations for each membrane model, generating a robust dataset for analysis. Each simulation encompassed 100 full oscillator cycles (including both decompression and compression phases), with the duration adjusted according to the specific frequency. Simulations were intentionally carried out for an equal number of ultrasound cycles (100 cycles) across different frequencies. This design ensures direct comparability of the mechanical response per cycle, independent of the absolute duration of the simulations, which is particularly relevant due to the non-equilibrium nature of these simulations. Consequently, observed frequency-dependent differences reflect intrinsic mechanical effects rather than artifacts related to differing simulation lengths.

Consistency across simulations was maintained by setting the wavefront parallel to the membrane surface, facilitating direct comparisons between different conditions. The intensity of the membrane's response to the US wave was quantified using the Short-Time Fourier Transform (STFT) method, as previously detailed (see supplementary material of reference [34] for a complete description and examples). In short, each property was standardized relative to its equilibrium value, resulting in fluctuations centered around zero. Time-resolved histograms and spectrograms of these normalized properties were calculated using STFT, with a Hann window function spanning 10 oscillations applied to each simulation. The time span of this window varied with the FUS frequency, ranging from 200 ns for 50 MHz to 2000 ns for 5 MHz, maintaining a 95 % overlap between consecutive windows. The resulting spectrograms were analyzed to extract the intensity at the fundamental frequency of the applied wave and its first harmonic. The sum of these intensities over time provides a measurement of the membrane's response to the US wave for each combination of frequency and amplitude. This process was repeated for all studied properties (area per lipid, curvature, thickness, and lipid-tail order parameters) across the range of US frequencies and overpressures employed. The logarithm of these intensities was taken to facilitate visualization, with higher values indicating stronger membrane responses to the US wave. Results were presented as heatmap matrices for each analyzed property, where each cell represents the membrane's response for a specific combination of ultrasound overpressure and frequency. Differences in behavior between membrane compositions were assessed by subtracting the response surfaces of different membrane types from one another. The statistical significance of these differences was evaluated using the Mann-Whitney *U* test [42], with a stringent significance level of 99.9 % applied throughout. This rigorous threshold ensures that only robust and reproducible differences are reported, minimizing the risk of false positives.

All simulations were performed using GROMACS 2021.5 [43–45], which was modified with in-house code to simulate the US wave. This custom code, also described in our previous work [34], is available upon request to facilitate reproducibility and further research. For data analysis, a suite of custom scripts was developed in Python 3.x, leveraging several powerful libraries for scientific computing and visualization. Specifically, NumPy [46] was used for general mathematical operations, MDAnalysis [47,48] for reading and processing GROMACS trajectories, SciPy [49] for Fourier analysis and statistical testing, and Matplotlib [50] for generating publication-quality graphs. All the simulations were performed at 298 K using a v-rescale [51] thermostat as implemented in the GROMACS package. Note that the use of the v-rescale thermostat was chosen explicitly to isolate the mechanical effects of ultrasound on the lipid bilayer, deliberately avoiding the potential thermal contributions and temperature-induced effects. Simulations performed without a thermostat showed unrealistic cooling towards absolute zero, reinforcing the necessity of thermostat usage to maintain physically meaningful simulation conditions.

The analysis focused on several key properties that provide insights into membrane structure and dynamics under US stimulation. The area per lipid was calculated using the method described by H. Bhatia and coworkers [52], offering a robust measure of membrane packing. The total curvature of the membrane was quantified following the approach of M.F. Ergüder and M. Deserno [53], allowing for the assessment of large-scale deformations induced by the US waves. Additionally, bilayer thickness and lipid order parameters were analyzed, as these properties are particularly sensitive to changes in membrane structure and fluidity. For these latter two properties, a local reference system was employed to account for the curved surface of the membrane when deformed by the US wave. This approach, detailed in our previous work [34], ensures accurate measurements even in the presence of significant membrane undulations.

Visualizations of the membranes and their trajectories were created using VMD [54] and FFmpeg [55] for generating animations of the dynamic processes. These visualizations provide illustrative insights into the complex, time-dependent behaviors observed in the simulations, aiding in the interpretation of the results. This comprehensive methodology allows for a systematic exploration of the effects of US waves on different lipid membranes across the selected range of frequencies and amplitudes.

3. Results

This study provides a detailed analysis of the effects of varying ultrasound parameters—specifically frequency and amplitude—on the mechanical deformation of lipid bilayers at the molecular level. The results provide valuable insights into the relationship between macroscopic ultrasound parameters and the nanoscale dynamics of lipid membranes. This study contributes to a deeper understanding of how specific ultrasound conditions affect membrane structure and behavior at the molecular level, aiming to be a reference for future research in this area.

As outlined in the methods section, the effects of a broad range of US frequencies (5–50 MHz) and overpressures (5–50 bar) were systematically examined across four distinct lipid compositions: POPC, POPE, POPG, and POPS. This comprehensive exploration aimed to generate a detailed "response map" that correlates US inputs with membrane behavior in different lipid environments. The chosen frequency range encompasses high-frequency ultrasound (HFUS, $\geq$10 MHz) and ultra-high-frequency ultrasound (UHFUS, >30 MHz), commonly employed in biomedical imaging applications such as dermatology and ophthalmology [56,57]. However, it differs from therapeutic ultrasound, where lower frequencies (~1–3 MHz) are typically used for deep tissue ablation [58]. Similarly, the applied overpressure range (5–50 bar, or 0.5–5 MPa) overlaps with pressure amplitudes encountered in B-mode ultrasound imaging (0.45–5.5 MPa) and pulsed-wave Doppler (0.67–5.3 MPa), while the upper bound aligns with the lower range of shock wave lithotripsy (5–15 MPa) [59]. It is crucial to acknowledge that the mechanical environment at the cellular or membrane level differs

significantly from macroscopic ultrasound conditions due to acoustic attenuation, wave reflection, and nonlinear interactions in biological tissues. Consequently, even when clinical and simulation conditions share similar frequency ranges, direct comparison is not feasible. Instead, our approach provides mechanistic insights into membrane-level effects under ultrasound exposure, complementing—but not replicating—experimental conditions in clinical applications.

On the other hand, at the nanoscale of our simulations, ultrasound waves were applied on the entire membrane region studied, as no experimental transducer is able to focus the mechanical perturbation in a narrower area. Thus, our simulations applied uniform acoustic perturbations across the entire bilayer region considered, effectively mimicking how ultrasound interacts with cellular membranes at the molecular level.

The analysis focused on multiple structural and dynamic responses of the membranes to the applied mechanical stress, including fluctuations in the APL as a quantitative measurement of membrane elasticity and packing, curvature change calculations to account for bending and undulation responses, thickness variations to assess compression and expansion dynamics, and order parameter alterations to probe lipid tail conformations and membrane fluidity.

In the following sections, the findings are presented, emphasizing how the interplay between US parameters and lipid composition governs membrane response.

3.1. Membrane response to ultrasound: structural deformations

The visual analysis of membrane trajectories reveals significant variations in membrane structure as a function of ultrasound frequency and pressure. Fig. 1 illustrates these effects for the POPC bilayer, showcasing membrane states during both decompression and compression phases of the ultrasound oscillation cycle. During the decompression step, membranes subjected to low-frequency (5 MHz) and high-pressure (50 bar) conditions exhibit extreme deformations. Notably, under these conditions, the membranes undergo a complete loss of their bilayer structure, elongating significantly in the direction of the applied force, which suggests that membrane integrity is compromised under these settings. At intermediate frequencies (25 MHz) and the same high pressure, the membrane shows pronounced curvature, indicating a substantial mechanical response.

In contrast, the compression phase demonstrates the membranes' ability to recover, with varying degrees of structural restoration depending on the applied ultrasound parameters. For instance, the membrane exposed to 5 MHz and 5 bar fully re-establishes its bilayer structure, albeit with a noticeable tilt relative to the XY plane of the simulation box. This tilt is likely a cumulative effect of repeated deformation cycles. Other membranes also revert to more compressed bilayer forms, with subtler variations that require further quantitative analysis.

The results observed for POPC are representative of the behavior seen in the other lipid compositions (POPE, POPG, and POPS). Across all compositions, the membranes exhibited similar patterns of deformation and recovery, indicating that the general response to varying ultrasound parameters is consistent, despite differences in lipid headgroup structures. This suggests that the fundamental mechanisms governing membrane response to ultrasound are largely independent of specific lipid composition, although slight variations in response intensity were noted, likely due to the differing physical properties of the individual lipids.

The stark contrast between decompression and compression states underscores the dynamic nature of membrane response to ultrasound stimulation. The frequency-dependent behaviours observed suggest that lower frequencies allow more time for lipid rearrangement within each cycle, leading to more pronounced deformations, particularly at 5 MHz. Conversely, higher frequencies, such as 50 MHz, result in more localized and less severe perturbations. Furthermore, the pressure-dependent responses highlight the mechanical thresholds of lipid bilayers. The extreme deformations observed at high pressures (50 bar) indicate a regime where the applied force exceed the membrane's intrinsic stability, potentially leading to transient pore formation or even membrane rupture. This phenomenon could have significant implications for ultrasound-mediated drug delivery or sonoporation techniques. Moreover, the recovery observed during the compression phase, particularly at lower pressures, highlights the remarkable self-healing properties of lipid membranes. This resilience is crucial for maintaining cellular integrity in biological systems subjected to mechanical stress.

3.2. Area per lipid

The analysis of APL across different membrane compositions under varying US conditions reveals complex response patterns that are highly dependent on both frequency and overpressure. A critical observation for all the lipid compositions considered is the identification of a parameter range, characterized by high overpressures and low frequencies, where membranes exhibit exceptionally high average APL values coupled with unusually large relative deviations. In these regions the membranes approach or exceed their structural stability limits, leading to the disruption of the characteristic bilayer topology. The precise boundaries of this instability zone vary with membrane composition.

Our results suggest that POPG and POPS have higher thresholds for instability, potentially due to the specific properties of their headgroups, which confer greater stability under ultrasound-induced stress. The instability thresholds vary with lipid composition. For POPC and POPE membranes, structural destabilization occurs at overpressures exceeding 30–35 bar and frequencies below 15–20 MHz, as seen in the upper

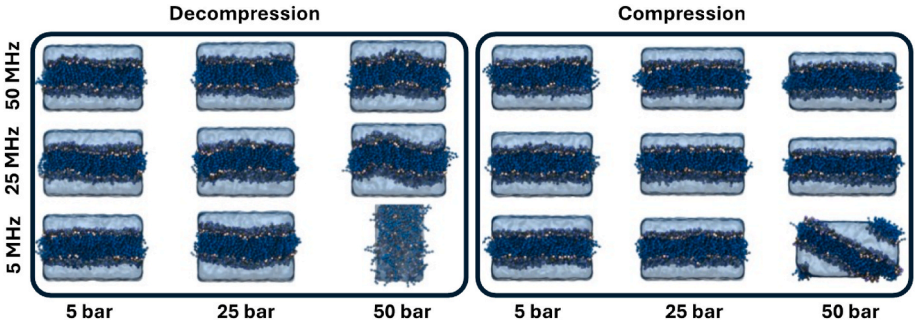

Fig. 1. Snapshots illustrating the deformation of POPC membrane deformation under varying ultrasound parameters. The matrix shows membrane responses at different frequencies (5 MHz, 25 MHz, 50 MHz) and overpressures (5 bar, 25 bar, 50 bar). Left panel: Membrane states during decompression. Right panel: Membrane states during compression. All snapshots were captured at the 100th oscillator cycle, illustrating the cumulative effects of prolonged ultrasound exposure on membrane structure.

panels of Fig. 2. Conversely, POPG and POPS membranes demonstrate greater resilience, with structural anomalies only emerging at overpressures above 40–45 bar and frequencies below 10 MHz, as shown in the lower panels. These observations suggest that POPG and POPS have higher thresholds for instability, potentially due to the specific properties of their headgroups, which confer greater stability under ultrasound-induced stress.

Notably, the transition into the instability region is not abrupt but gradual, with a visible gradient of increasing APL and relative deviations as conditions approach the critical zone. This gradual progression indicates that the membranes begin to destabilize progressively as they approach the limits of their structural integrity. However, POPG and POPS membranes, despite their overall greater stability exhibit a sharper transition into the instability region compared to POPC and POPE. This sharper transition suggest amore sudden structural failure once critical conditions are met, hinting at distinct stability characteristics likely influenced by the negatively charged headgroups of POPG and POPS compared to the zwitterionic nature of POPC and POPE.

Across all studied compositions, a consistent relationship is observed between frequency and the overpressure threshold for membrane failure. As depicted in the heatmaps, lower frequencies require lower overpressures to induce instability, while higher frequencies allow membranes to withstand greater overpressures before exhibiting signs of structural breakdown. This trend highlights the interplay between frequency and overpressure in governing membrane stability, with lower frequencies enabling more time for lipid rearrangement within each cycle, thereby facilitating more extreme deformations.

Beyond these critical regions, the response surfaces exhibit remarkably consistent trends across all lipid compositions. The behavior of average APL reveals a complex dependence on both frequency and overpressure. At low overpressures, APL generally increases with increasing frequency, indicating that the membrane expands more at higher frequencies. However, this trend reverses at high overpressures, where the highest APL values are observed at the lowest frequencies. This inversion of the frequency-dependence underscores a critical interplay between frequency and overpressure in determining membrane response. It suggests that at high overpressures, lower frequencies allow for more extreme membrane deformations, possibly due to longer time periods for lipid rearrangement within each ultrasound cycle.

The relative deviations in APL show a distinct pattern, forming a U-shaped profile along the overpressure axis. The highest deviations occur both in the instability regions at high overpressures and low frequencies, and at very low overpressures across all frequencies. This pattern indicates that membranes exhibit the most variable APL under extreme conditions, either at very low or very high stress, with a zone of relative stability in between.

Fig. 3 further elucidates the compositional effects by presenting pairwise difference matrices of APL response surfaces for the four lipid types studied. The matrices illustrate the differences in APL responses between each pair of lipid compositions across the range of ultrasound conditions. POPC consistently exhibits the highest APL values among all lipid types, particularly under high-frequency and high-overpressure conditions, as indicated by the predominance of red areas in the comparisons involving POPC. This suggests that POPC membranes are more prone to expansion under these conditions, potentially leading to greater membrane destabilization.

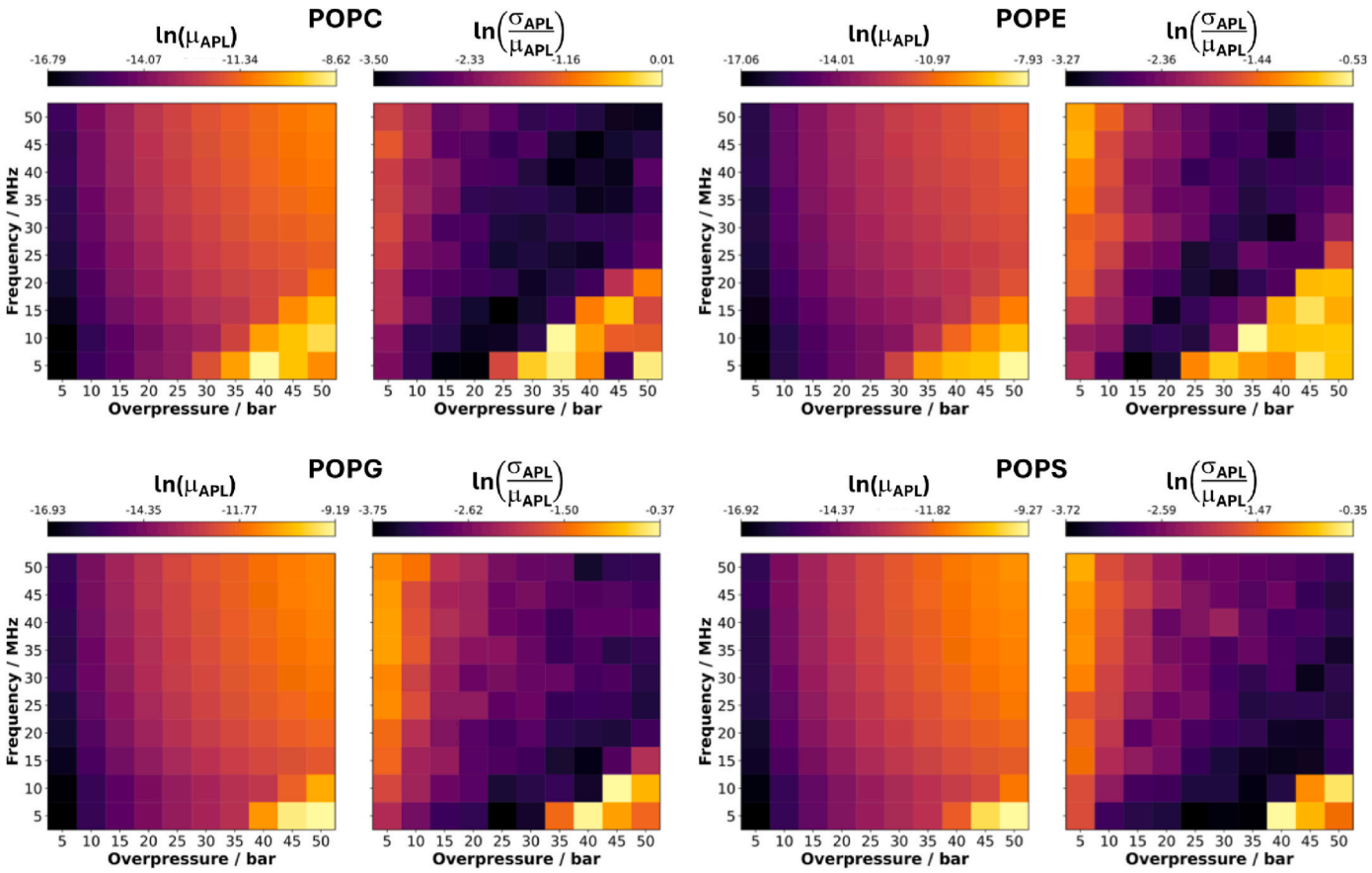

Fig. 2. Area per lipid (APL) response for the studied systems under varying ultrasound conditions. Two heatmaps are plotted for each lipid bilayer: Logarithm of mean APL, $\ln(/\mu_{APL})$, showing average membrane expansion or compression (left); and Logarithm of relative APL fluctuations, $\ln(\sigma_{APL}//\mu_{APL})$, indicating the magnitude of APL variations relative to its average value (right). Color scale: Blue indicates lower values, red higher values. This logarithmic representation enhances visibility of subtle variations across different ultrasound parameter regimes. (For interpretation of the references to colour in this figure legend, the reader is referred to the Web version of this article.)

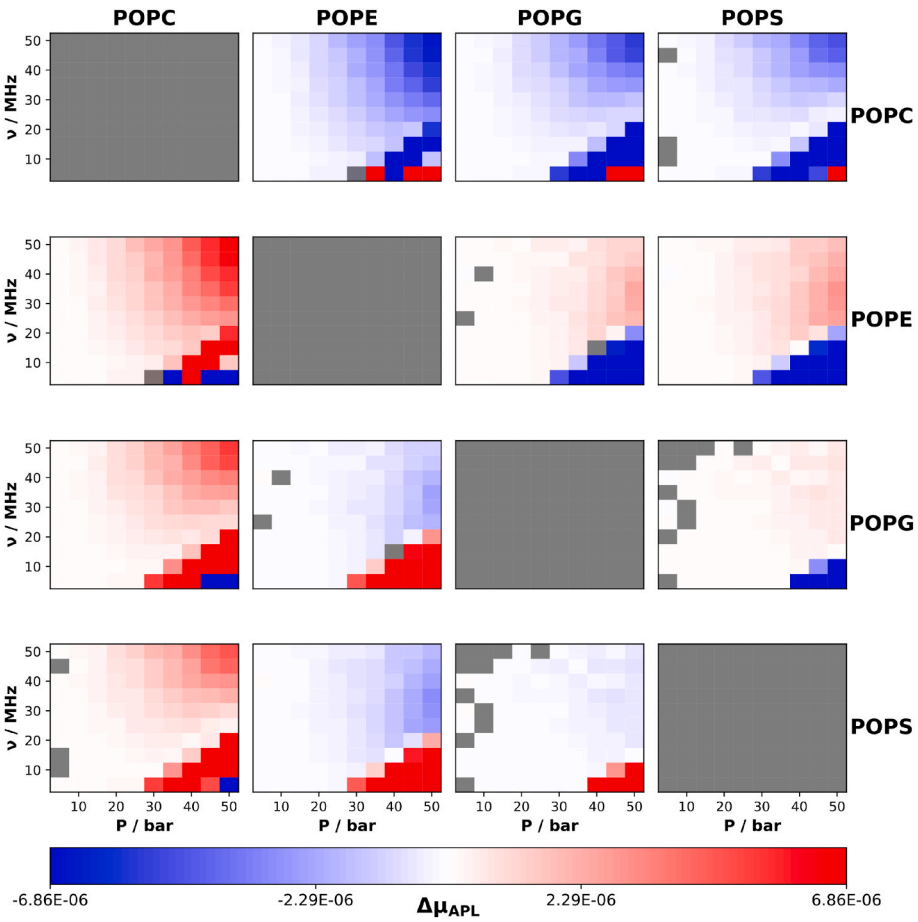

Fig. 3. Pairwise difference matrix of area per lipid (APL) response surfaces for POPC, POPE, POPG, and POPS membranes under varying ultrasound conditions. Each subplot shows ΔAPL (column lipid minus row lipid) across frequencies (ν) and overpressures (P). Red indicates positive differences, blue negative, with intensity proportional to magnitude. Gray areas represent differences not statistically significant at the 99.9 % confidence level. (For interpretation of the references to colour in this figure legend, the reader is referred to the Web version of this article.)

In contrast, POPE shows the lowest APL responses across the studied conditions, particularly when compared to POPC, where blue regions in the heatmaps dominate. This indicates that POPE membranes are generally more resistant to expansion and maintain a more stable structure under ultrasonic stress. POPG and POPS show intermediate behaviors, with slight differences observed between them. Notably, POPS tends to exhibit slightly higher APL values than POPG under high frequencies and overpressure conditions, as reflected by the subtle red regions in the corresponding heatmap. The relatively small differences between POPG and POPS suggest that these lipids, while distinct in their chemical properties, behave similarly under the applied ultrasound conditions.

These findings underscore the critical role of lipid composition in determining membrane behavior under ultrasonic stress. It is important to note that our simulations explicitly impose mechanical perturbations through ultrasound waves, driving membranes far from thermodynamic equilibrium, where classical definitions of thermodynamic phases (solid or fluid) are not rigorously applicable. Instead, membranes dynamically adopt transient structural states characterized by continuous rearrangements. Nevertheless, the clear trend observed for the area per lipid response (POPC $>$ POPS $\geq$ POPG $>$ POPE) can be rationalized by intrinsic lipid properties: the large, extensively hydrated headgroup of POPC leads to looser packing, greater flexibility, and thus higher susceptibility to deformation. In contrast, negatively charged POPG and POPS lipids exhibit stronger cohesion through electrostatic interactions with counterions and hydration shells, reducing their susceptibility. POPE membranes, with their compact, minimally hydrated headgroups, demonstrate the highest mechanical stability and lowest susceptibility to deformation under ultrasound stress. Therefore, understanding the interplay between lipid composition and ultrasound parameters is crucial for designing targeted biomedical applications aimed at selective membrane disruption.

3.3. Curvature

The response of membrane curvature to variations in US parameters (Fig. 4) reveals patterns distinct from those observed for APL. A consistent finding across all lipid compositions is that the lowest overpressure exerts minimal effect on the membranes regardless of the frequency applied. This minimal response at low overpressures is coupled with high relative deviations, suggesting increased variability in curvature responses under these conditions. Such variability may indicate heterogeneous deformation across the membrane, with some regions exhibiting more pronounced bending than others under mild mechanical stress.

Regions of curvature instability, similar to those observed in APL measurements, are identified at high overpressures and low frequencies. These regions are characterized by abrupt changes in curvature in response to small variations in US parameters, indicating heightened sensitivity of the membrane structure under these specific conditions. The sharp changes in curvature suggest that the membrane is approaching a threshold where the applied mechanical forces exceed its intrinsic stability, potentially leading to significant structural perturbations or failure.

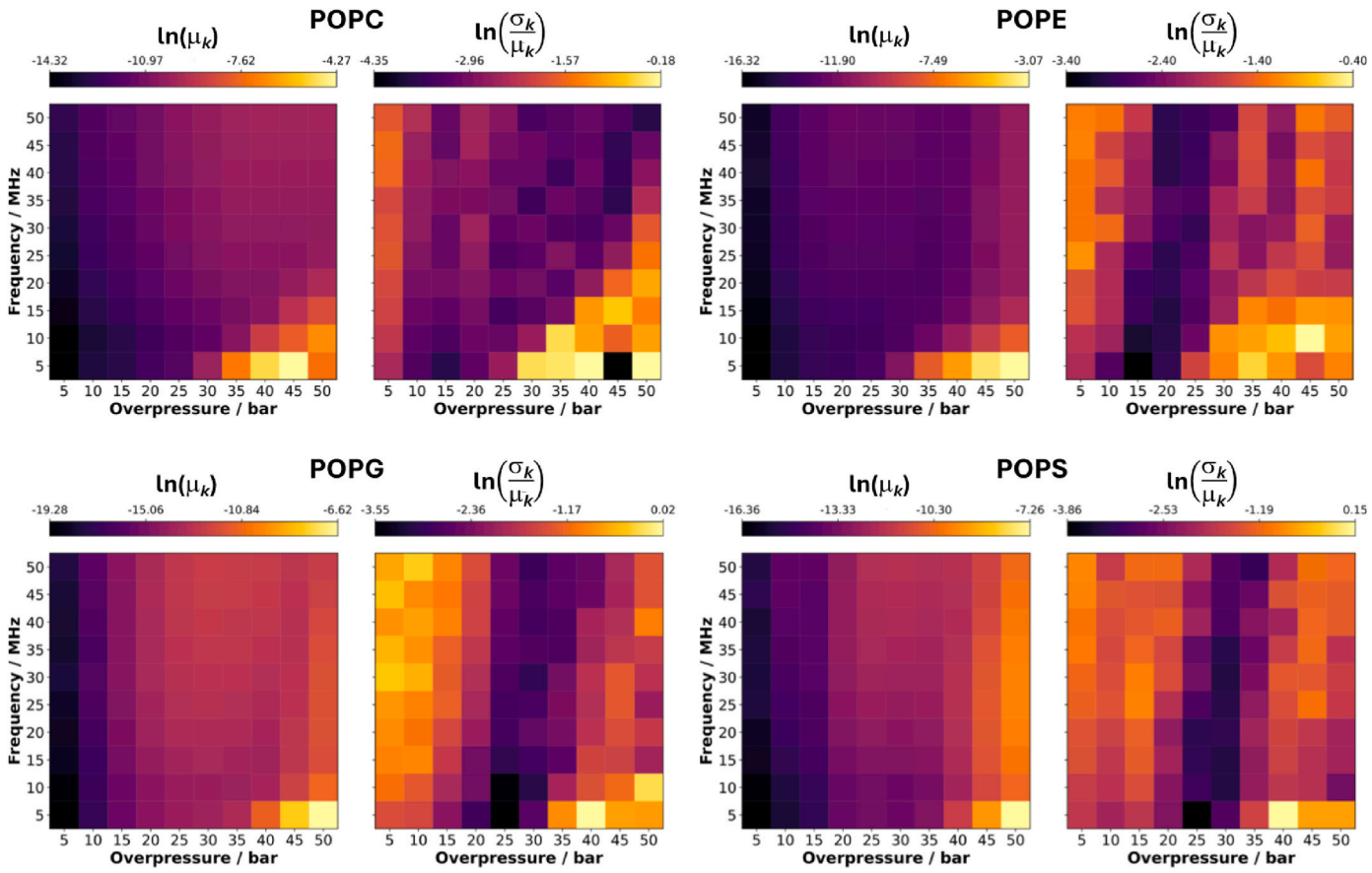

Fig. 4. Curvature (k) response for the studied systems under varying ultrasound conditions. Two heatmaps are plotted for each lipid bilayer: Logarithm of mean curvature, $\ln(\mu_k)$, showing average membrane expansion or compression (left); and Logarithm of relative k fluctuations, $\ln(\sigma_k/\mu_k)$, indicating the magnitude of k variations relative to its average value (right). Color scale: Blue indicates lower values, red higher values. This logarithmic representation enhances visibility of subtle variations across different ultrasound parameter regimes. (For interpretation of the references to colour in this figure legend, the reader is referred to the Web version of this article.)

As for APL, the relative curvature fluctuations exhibit a U-shaped behavior across the overpressure axis. High fluctuations are observed at both low and high overpressures, with a zone of reduced fluctuations at intermediate values, particularly between 15 and 35 bar. However, a significant increase in fluctuation is observed above 35–40 bar, indicating the onset of instability. This non-monotonic pattern suggests a complex interplay between US parameters and membrane curvature, where both very low and very high mechanical stresses lead to more variable curvature responses. The initial high fluctuations at low overpressures likely result from the membrane's flexibility, allowing it to bend without fully committing to a deformation pathway, while the increased fluctuations at higher overpressures may reflect the onset of structural failure as the membrane's capacity to absorb stress is exceeded.

Further insights into the effects of lipid composition on curvature response are provided by the pairwise difference matrices in Fig. 5. These matrices reveal significant variations across all examined membrane compositions, underscoring the crucial role of membrane composition in determining the bilayers' response to ultrasound-induced mechanical deformation.

POPC membranes exhibit a distinct pattern, characterized by a higher curvature perturbation responses across most of the frequency and overpressure range, as indicated by the predominance of red in the first column of Fig. 5. This suggests that POPC membranes are generally more susceptible to bending under ultrasound stress, particularly at higher overpressures and lower frequencies. However, a small region at the highest overpressures and lowest frequencies shows that the curvature of POPC is lower than that of other bilayers, indicating a potential stabilizing effect under these extreme conditions.

POPE membranes display a more complex pattern of differences when compared to other lipid compositions. For instance, compared to POPG, POPE shows an enhanced curvature response at high overpressures and very low frequencies, as evidenced by the red region in the bottom right of their comparison matrix. This suggests that POPE membranes might undergo more pronounced bending under these specific conditions. The comparison between POPE and POPS reveals a similar behavior at low frequencies, with POPE showing greater curvature at these low frequencies and overpressures, while POPS exhibits a higher curvature response at higher frequencies and overpressures.

POPG and POPS membranes demonstrate similar behavior patterns, consistent with their APL analysis results. Significant differences between these two compositions are primarily observed at the largest overpressure values, with more curvature of POPG at the lowest frequencies and more curvature of POPS at frequencies above 20 MHz. This indicates that while both lipids share similar structural characteristics, their responses to ultrasound stress diverge subtly depending on the specific combination of frequency and overpressure.

3.4. Thickness

The response surfaces for membrane thickness (Fig. 6) demonstrate patterns that share similarities with the membrane curvature but also exhibit distinct characteristics. As observed in previous analyses, the influence of frequency on membrane thickness is minimal at the lowest overpressure, where the relative fluctuations are high. These fluctuations suggest a lack of uniformity in how the membrane responds to

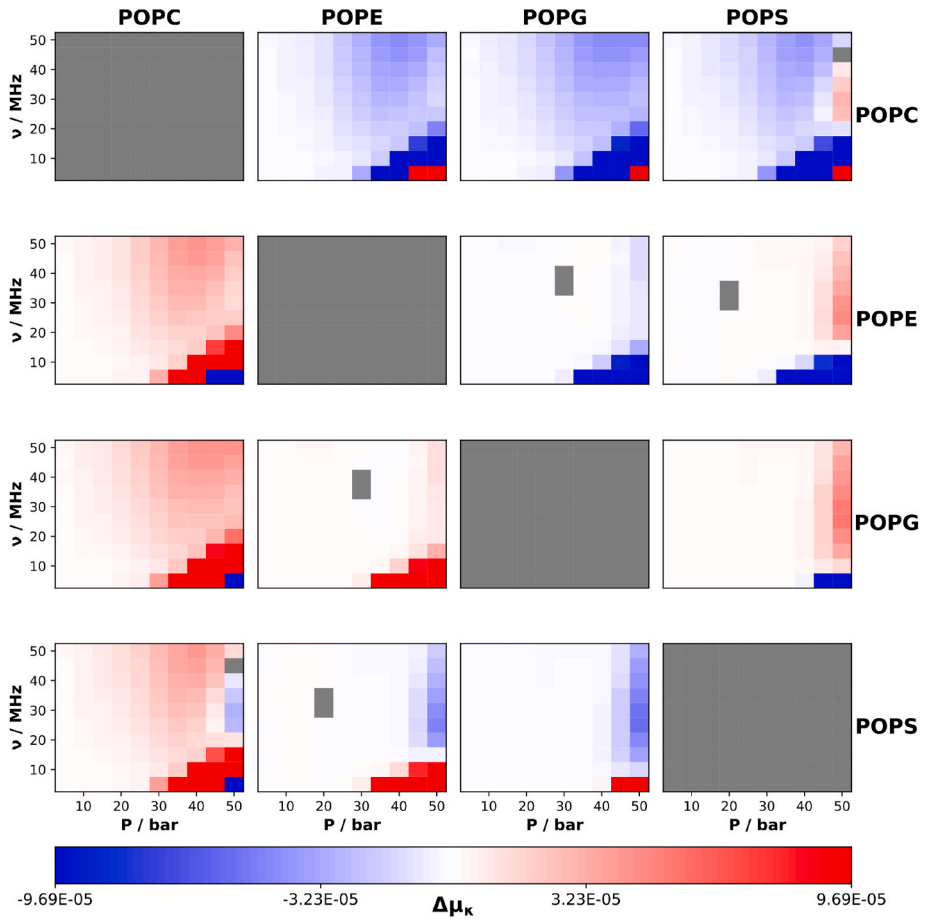

Fig. 5. Pairwise difference matrix of curvature (k) response surfaces for POPC, POPE, POPG, and POPS membranes under varying ultrasound conditions. Each subplot shows $\Delta\mu_k$ (column lipid minus row lipid) across frequencies (ν) and overpressures (P). Red indicates positive differences, blue negative, with intensity proportional to magnitude. Gray areas represent differences not statistically significant at the 99.9 % confidence level. (For interpretation of the references to colour in this figure legend, the reader is referred to the Web version of this article.)

ultrasound at low mechanical stress, likely reflecting heterogeneous compression or expansion across different regions of the bilayer.

Instability regions, marked by significant changes in membrane thickness, are consistently identified at high overpressures and low frequencies across all lipid compositions. These regions correspond closely to those observed for curvature and APL, indicating that these properties are governed by similar underlying mechanisms when subjected to intense ultrasound conditions. The U-shaped behavior of thickness fluctuations, characterized by high variability at both low and high overpressures and a zone of reduced fluctuations at intermediate values, further supports the idea that extreme mechanical stresses—whether too low or too high—induce more variable and less predictable membrane responses.

The pairwise difference matrices for membrane thickness (Fig. 7) reveal a more complex landscape of responses across various lipid compositions when subjected to ultrasound. Compared to the differences observed in APL and curvature, the responses in thickness show more intricate trends, particularly in how different lipid compositions influence the bilayer's ability to maintain or alter its thickness under mechanical stress.

A striking feature of this analysis is the presence of multiple trends when comparing any two specific membrane types, with many differences being statistically significant across almost the entire parametric space. This underscores the profound impact of lipid composition on membrane thickness in response to ultrasound. The POPC membrane shows the most pronounced differences when compared to other lipid types, as evidenced by the intense red and blue regions in the POPC comparison matrices (first column of Fig. 7). These differences are particularly marked at higher overpressures, where the thickness of POPC membranes diverges significantly from that of other lipids.

The comparison between POPC and POPE reveals several transitions with alternating sign in the thickness differences as the frequency increases at high overpressures. This suggests a complex interplay between these two lipid types, where POPC membranes are generally thicker at lower frequencies, but POPE membranes surpass this thickness at higher frequencies and overpressures. In the comparison between POPC and POPS, a similar pattern is observed, but with a single change of sign—POPC exhibits greater thickness at low frequencies, while POPS becomes thicker at frequencies above approximately 20 MHz.

The comparison between POPC and POPG shows a clearer trend, with POPC consistently producing thicker bilayers regardless of the pressure and frequency conditions. This indicates that POPC's intrinsic properties favor a more robust bilayer structure that resists compression across a wide range of ultrasound parameters.

Comparisons between other pairs of lipids reveals different patterns. POPE and POPG exhibit similar thickness responses at overpressures lower than 40 bar, but at higher overpresures, POPE bilayers become significantly thicker than those of POPG, regardless the frequency. This suggests that POPE membranes are more resistant to thinning under high mechanical stress. The differences in bilayer thickness between POPE and POPS are highly dependent on the frequency at high overpressures but remain almost negligible at lower pressures, indicating that frequency plays a crucial role in determining the relative thickness

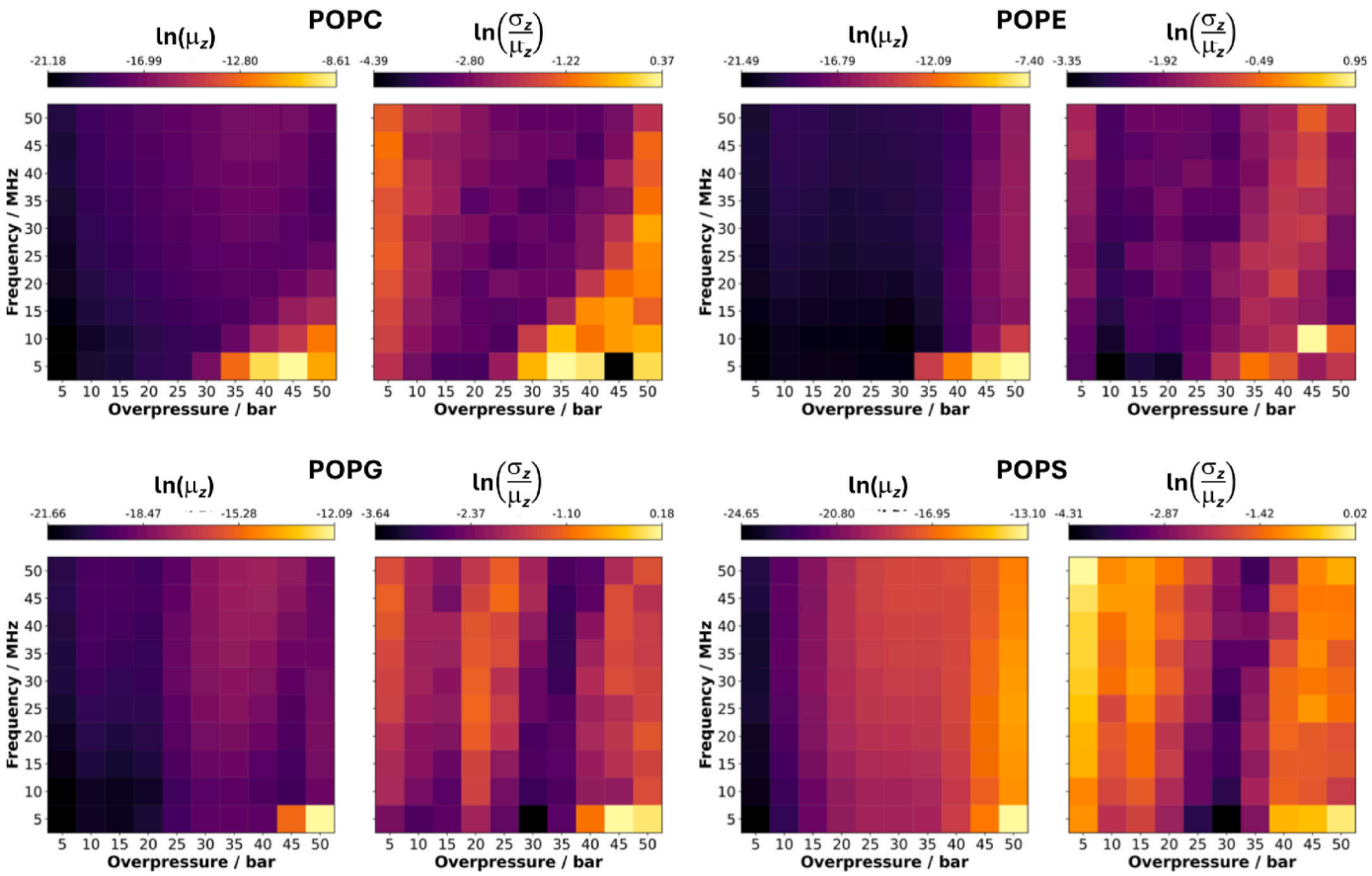

Fig. 6. Thickness (z) response for the studied systems under varying ultrasound conditions. Two heatmaps are plotted for each lipid bilayer: Logarithm of mean thickness, ln(μz), showing average membrane expansion or compression (left); and Logarithm of relative z fluctuations, $\ln(\sigma_z/\mu_z)$, indicating the magnitude of z variations relative to its average value (right). Color scale: Blue indicates lower values, red higher values. This logarithmic representation enhances visibility of subtle variations across different ultrasound parameter regimes. (For interpretation of the references to colour in this figure legend, the reader is referred to the Web version of this article.)

of these membranes under stress. In contrast, the thickness of POPG bilayers is generally lower than that of POPS bilayers at high overpressures, except at very low frequencies where POPG exhibits greater thickness. At overpressures below 40 bar, the differences between these two lipid types are minimal, highlighting the role of both frequency and overpressure in modulating membrane thickness.

3.5. Order parameters

The order parameters of lipid membranes, as shown in Fig. 8, exhibit a systematic response to varying ultrasound conditions, highlighting notable differences across the studied bilayer compositions. A consistent trend is observed, where order parameter values increase with rising overpressure and decreasing frequency. This trend is particularly evident under conditions of low frequency (5–20 MHz) and high overpressure (35–50 bar), where the lipid tails exhibit a higher degree of alignment, suggesting increased membrane rigidity or compression. These findings indicate that under these specific ultrasound conditions, the membranes are more structurally ordered. Conversely, the lowest order parameters are found at high frequencies (40–50 MHz) and low overpressures (5–15 bar), which correlates with a state of enhanced membrane fluidity or expansion, likely due to the reduced mechanical stress and higher vibrational frequencies.

The rapid changes in order parameters observed within the low-frequency range (5–20 MHz), as pressure increases, underscore a transition region where the membranes undergo significant structural reorganization. This transition, marked by a shift from low to high order parameter values, reflects the membranes' response to the increasing mechanical stress, which induces greater lipid tail alignment as the membrane compresses under the ultrasound wave. In contrast, at high frequencies and low pressures, the membranes demonstrate increased disorder, which may be indicative of enhanced membrane fluidity or decreased packing density.

Fluctuations in the order parameters follow a distinct and reproducible pattern across the different lipid compositions. The highest fluctuations in the order parameters (bright yellow regions) are observed at high frequencies (40–50 MHz) and low overpressures (5–15 bar), where membranes appear more dynamic and less stable. As overpressure increases and frequency decreases, these fluctuations gradually diminish, with the most stable configurations (indicated by the lowest fluctuations, dark blue areas) occurring at low frequencies (5–20 MHz) and high overpressures (35–50 bar). This pattern is consistent across the different lipids, although the fluctuations seem higher for POPG bilayers compared to other membrane models, indicating that POPG may be more prone to dynamic structural changes under these specific conditions (Fig. 8).

The comparative analysis of different lipid compositions, as depicted in the pairwise difference matrices in Fig. 9 and Fig. S7, reveals significant compositional effects on the order parameters. The POPC membranes consistently demonstrate a larger response in the SN1-A order parameter, compared to other lipid bilayers, particularly when contrasted with POPE. This difference is most pronounced under conditions of high overpressure and low frequency, where POPC exhibits significantly greater lipid tail alignment. Interestingly, the smallest differences

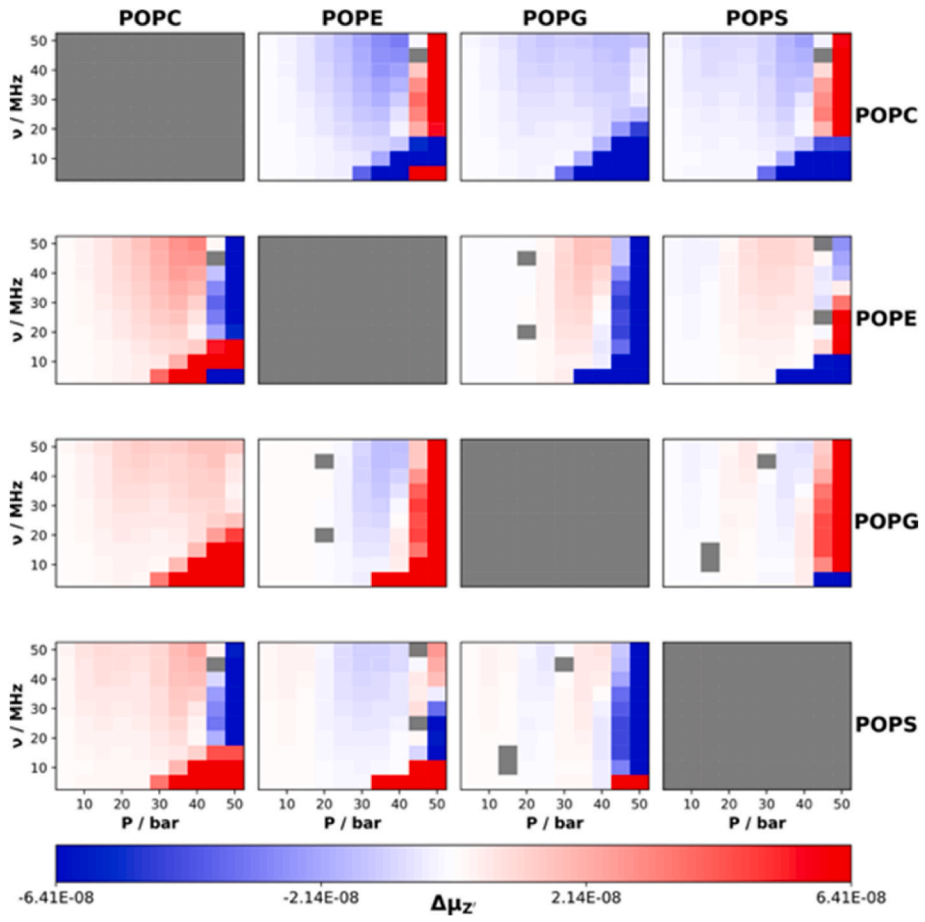

Fig. 7. Pairwise difference matrix of thickness (z) response surfaces for POPC, POPE, POPG, and POPS membranes under varying ultrasound conditions. Each subplot shows Δμz (column lipid minus row lipid) across frequencies (ν) and overpressures (P). Red indicates positive differences, blue negative, with intensity proportional to magnitude. Gray areas represent differences not statistically significant at the 99.9 % confidence level. (For interpretation of the references to colour in this figure legend, the reader is referred to the Web version of this article.)

between POPC and the other membranes occur at higher frequencies (~40 MHz), where the order parameter values tend to converge, suggesting a uniform response across different lipid types under these specific conditions.

In contrast, POPE membrane displays lower order parameters compared to POPG and POPS, except at very low overpressures where differences are minimal. Under conditions of low frequencies and high overpressures, POPE membrane show higher order parameters than those of POPG and POPS, indicating a greater degree of lipid tail alignment under these conditions. Despite their similar aliphatic tail structures, POPG and POPS exhibit subtle yet significant differences in their order parameter responses, particularly under extreme ultrasound conditions (very high overpressure and very low frequency). Here, POPG tends to show slightly higher order than POPS, though these differences are relatively minor and concentrated in specific regions of the parameter space.

Furthermore, the response surfaces for other order parameters, as detailed in the Supporting Fig. S7, largely mirror the behaviors discussed earlier. However, a noteworthy deviation is noted in the POPC membrane, where its response near instability regions becomes less pronounced compared to other lipid types. This suggests a potential convergence in membrane behavior under extreme conditions, with POPC exhibiting unique structural properties that differentiate it from other membranes.

As the analysis progresses along down the aliphatic tail of the lipid molecules, an increasing number of values in the order parameter matrices lack statistical significance, particularly in the lower regions of the tails. This trend indicates a convergence in the behavior of the studied membranes, implying that the physical responses of the bilayers become more uniform across lipid types in these regions. This could be due to similar packing or mobility characteristics in the lower parts of the lipid molecules, suggesting a shared structural response to ultrasound across different membrane compositions.

4. Conclusions

This study provides a detailed examination of how ultrasound frequency and overpressure influence the structural and mechanical properties of lipid bilayers composed of POPC, POPE, POPG, and POPS. These lipids, which are representative of various cellular environments including mammalian, bacterial, and cancerous cells, were chosen to explore membrane dynamics under mechanical stress. By systematically varying both the frequency (5–50 MHz) and overpressure (5–50 bar) across these four distinct lipid compositions, this work aimed to map out the detailed response of these membranes to mechanical perturbations. The results underscore the critical role of lipid composition in determining how membranes respond to ultrasound-induced perturbations, revealing complex behaviors that vary significantly depending on both the lipid type and the specific ultrasound conditions applied.

A key finding from this study is the consistent relationship observed between ultrasound parameters and membrane behavior. Lower frequencies combined with higher overpressures generally induced more pronounced structural deformations across all lipid types. This was particularly evident in the analysis of area per lipid (APL) and curvature,

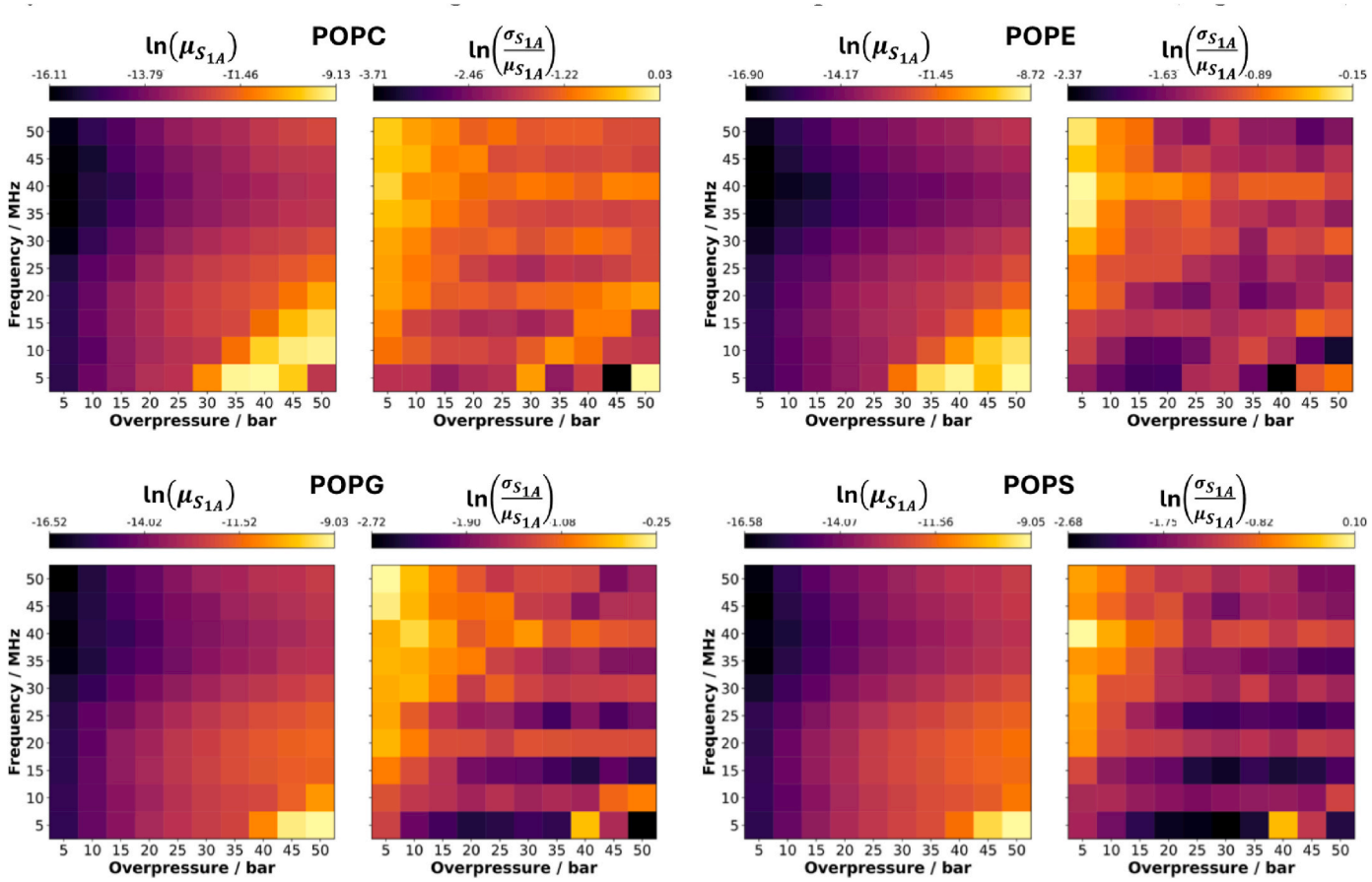

Fig. 8. Order parameter (OP) for the response of the first bead of SN1 of the studied systems under varying ultrasound conditions. Two heatmaps are plotted for each lipid bilayer: Logarithm of mean OP, $\ln(\mu_{S1A})$, showing average membrane expansion or compression (left); and Logarithm of relative OP fluctuations, $\ln(\sigma_{S1A}/\mu_{S1A})$, indicating the magnitude of OP variations relative to its average value (right). Color scale: Blue indicates lower values, red higher values. This logarithmic representation enhances visibility of subtle variations across different ultrasound parameter regimes. (For interpretation of the references to colour in this figure legend, the reader is referred to the Web version of this article.)

where specific combinations of frequency and overpressure led to significant deviations from equilibrium values, indicating that the membranes were approaching or exceeding their structural stability limits. For example, membranes composed of POPC and POPE were found to destabilize at overpressures exceeding 30–35 bar and frequencies below 15–20 MHz. In contrast, POPG and POPS membranes demonstrated greater resilience, with structural anomalies emerging only at overpressures above 40–45 bar and frequencies below 10 MHz. The sharper transitions into instability observed in POPG and POPS suggest a more sudden structural failure under extreme conditions, likely influenced by the specific chemical properties of their lipid headgroups.

The study also highlighted the existence of instability regions where membranes are particularly susceptible to disruption. These regions, characterized by high APL values and large relative deviations, were more pronounced in POPC and POPE membranes. In contrast, POPG and POPS exhibited a more gradual approach to instability, although when they did destabilize, the change was more abrupt. This behavior is likely due to the unique stability characteristics conferred by the negatively charged headgroups of POPG and POPS, compared to the zwitterionic nature of POPC and POPE. The findings suggest that the physical and chemical properties of lipid headgroups play a significant role in influencing membrane stability and response to mechanical stress.

The curvature and thickness of the membranes also varied significantly with ultrasound conditions, with similar patterns to those observed for APL. Membrane thickness, for instance, displayed a U-shaped response to changes in overpressure, with the most stable configurations occurring at intermediate pressures, while extreme low or high pressures led to greater variability and instability. The differences in thickness and curvature responses between the lipid types were particularly pronounced at higher overpressures, where POPC membranes consistently showed more significant deviations compared to POPE, POPG, and POPS. This suggests that POPC membranes are more prone to bending and compression under intense ultrasound stress, potentially leading to greater susceptibility to mechanical disruption.

The order parameter analysis provided additional insights into the molecular-level changes occurring within the lipid bilayers under ultrasound stress. As with the other structural properties, the order parameters exhibited a clear dependence on both frequency and overpressure. Lower frequencies and higher overpressures led to increased lipid tail alignment, indicating greater membrane rigidity. Conversely, higher frequencies and lower overpressures resulted in more disordered, fluid membrane states. Notably, POPC membranes consistently exhibited higher order parameter values under these conditions, suggesting that they are more susceptible to becoming rigid and potentially less flexible under stress. In contrast, POPE membranes showed lower order parameters, indicating a tendency to maintain a more fluid and flexible structure under similar conditions. POPG and POPS, while similar in their general behavior, displayed subtle differences in response, particularly under extreme conditions, where POPG exhibited slightly higher order than POPS.

The sharper instability in POPG and POPS membranes may be particularly relevant when considering the biological contexts in which these lipids are commonly found. POPG is prevalent in bacterial membranes, and POPS is often exposed on the outer leaflet of cancer cell

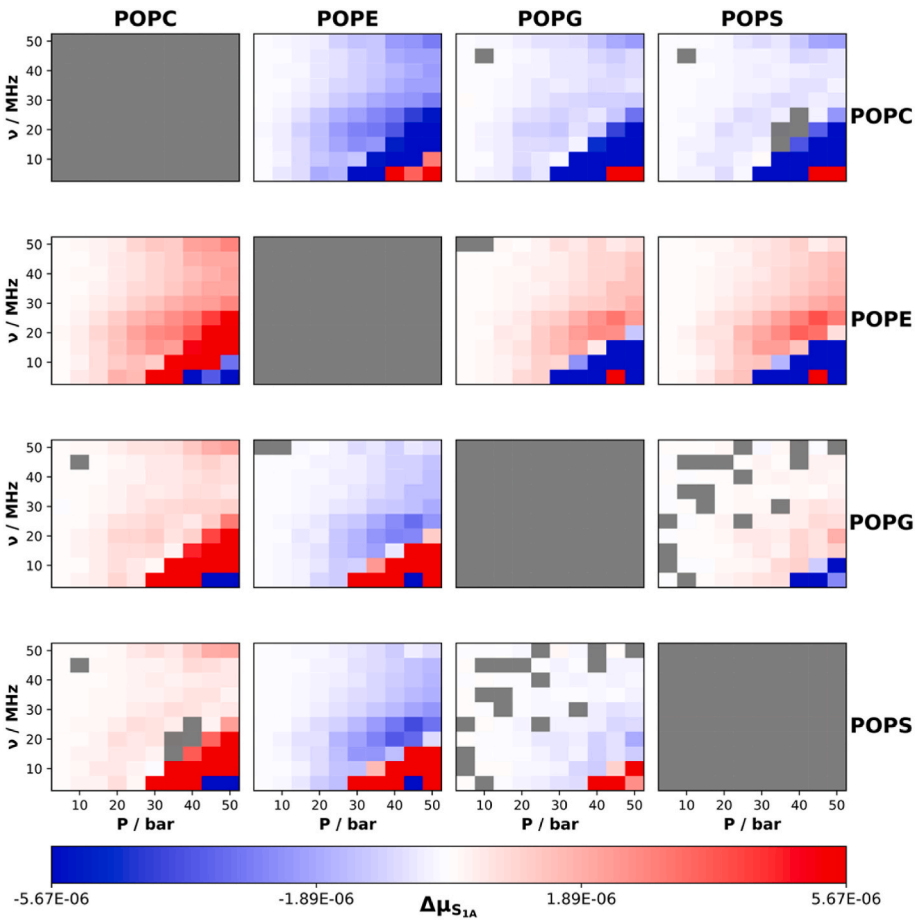

Fig. 9. Pairwise difference matrix of Order parameter (OP) for the response of the first bead of SN1 of the studied systems under varying ultrasound conditions. Each subplot shows $\Delta\mu_{S1A}$ (column lipid minus row lipid) across frequencies (ν) and overpressures (P). Red indicates positive differences, blue negative, with intensity proportional to magnitude. Gray areas represent differences not statistically significant at the 99.9 % confidence level. (For interpretation of the references to colour in this figure legend, the reader is referred to the Web version of this article.)

membranes. The distinct stability patterns observed under ultrasonic stress might reflect an adaptive advantage in these environments, where the ability to withstand certain mechanical stresses is crucial. However, when subjected to extreme conditions, the sharp decline in stability observed in these lipids could be exploited therapeutically, particularly in strategies aimed at selectively targeting bacterial infections or cancer cells through ultrasound-based techniques.

This study not only enhances the understanding of how ultrasound parameters influence membrane structure but also opens avenues for further investigation. Future research could explore how lipid mixtures, more representative of actual biological membranes, respond to ultrasound. Additionally, the impact of embedded peptides or proteins within these membranes should be studied to understand their influence on structural and mechanical responses. Moreover, the effects of temperature changes, often associated with ultrasound treatments, warrant investigation to provide a more comprehensive picture of membrane behavior in therapeutic contexts. Such studies will be crucial for optimizing the use of ultrasound in medical applications, ensuring both efficacy and safety in treatments that target cell membranes. By identifying the conditions under which different lipid compositions are more susceptible to mechanical disruption, this study contributes valuable insights into the broader field of membrane biophysics and the potential for ultrasound-based therapeutic interventions.

CRediT authorship contribution statement

Alexandre Blanco-González: Writing – review & editing, Writing – original draft, Validation, Methodology, Formal analysis, Data curation, Conceptualization. **Ángel Piñeiro:** Writing – review & editing, Writing – original draft, Supervision, Resources, Project administration, Investigation, Funding acquisition, Conceptualization. **Rebeca García-Fandiño:** Writing – review & editing, Writing – original draft, Validation, Resources, Project administration, Investigation, Funding acquisition, Conceptualization.

Declaration of generative AI and AI-assisted technologies in the writing process

During the preparation of this work the authors used chatGPT4o from OpenAI and Claude 3.5 Sonnet from Anthropic in order to improve language and readability. After using these tools, the authors reviewed and edited the content as needed and take full responsibility for the content of the publication.

Acknowledgements

This work was supported by the Spanish Agencia Estatal de Investigación (AEI) and the ERDF (PDC2022-133402-I00, PID2022-141534OB-I00 and CNS2023-144353), by Xunta de Galicia and the ERDF (06_IN606D_2021_2600276) and by Interreg VI-B SUDOE (). This work has received financial support from the Xunta de Galicia (Centro de investigación do Sistema universitario de Galicia accreditation 2023–2027, ED431G 2023/03) and the European Union (European Regional Development Fund - ERDF). A.B.G thanks Xunta de Galicia and

Axencia Galega de Innovación for his predoctoral contract (06_IN606D_2021_2600276) All calculations were carried out at the Centro de Supercomputación de Galicia (CESGA).

Appendix A. Supplementary data

Supplementary data to this article can be found online at https://doi.org/10.1016/j.abb.2025.110523.

References

[1] B. Stieger, J. Steiger, K.P. Locher, Membrane lipids and transporter function, Biochim. Biophys. Acta - Mol. Basis Dis. 1867 (2021) 166079, https://doi.org/10.1016/j.bbadis.2021.166079.

[2] V. Corradi, B.I. Sejdiu, H. Mesa-Galloso, H. Abdizadeh, S.Y. Noskov, S.J. Marrink, D.P. Tieleman, Emerging diversity in lipid-protein interactions, Chem. Rev. 119 (2019) 5775–5848, https://doi.org/10.1021/acs.chemrev.8b00451.

[3] R. Nussinov, C.J. Tsai, H. Jang, Ras assemblies and signaling at the membrane, Curr. Opin. Struct. Biol. 62 (2020) 140–148, https://doi.org/10.1016/j.sbi.2020.01.009.

[4] P. Sens, J. Plastino, Membrane tension and cytoskeleton organization in cell motility, J. Phys. Condens. Matter 27 (2015) 273103, https://doi.org/10.1088/0953-8984/27/27/273103.

[5] D. Conde-Torres, A. Blanco-González, A. Seco-González, F. Suárez-Lestón, A. Cabezón, P. Antelo-Riveiro, Á. Piñeiro, R. García-Fandiño, Unraveling lipid and inflammation interplay in cancer, aging and infection for novel theranostic approaches, Front. Immunol. 15 (2024) 1320779, https://doi.org/10.3389/fimmu.2024.1320779.

[6] A. Blanco-González, Á. Piñeiro, R. García-Fandiño, Unravelling hierarchical levels of structure in lipid membranes, Comput. Struct. Biotechnol. J. 20 (2022) 2798–2806, https://doi.org/10.1016/j.csbj.2022.05.042.

[7] C. Sohlenkamp, O. Geiger, Bacterial membrane lipids: diversity in structures and pathways, FEMS Microbiol. Rev. 40 (2015) 133–159, https://doi.org/10.1093/femsre/fuv008.

[8] T. Harayama, H. Riezman, Understanding the diversity of membrane lipid composition, Nat. Rev. Mol. Cell Biol. 19 (2018) 281–296, https://doi.org/10.1038/nrm.2017.138.

[9] V.A.M. Gold, A. Robson, H. Bao, T. Romantsov, F. Duong, I. Collinson, The action of cardiolipin on the bacterial translocon, Proc. Natl. Acad. Sci. U. S. A. 107 (2010) 10044–10049, https://doi.org/10.1073/pnas.0914680107.

[10] M. Pan, C. Qin, X. Han, Lipid metabolism and lipidomics applications in cancer research, in: Adv. Exp. Med. Biol., Springer, 2021, pp. 1–24, https://doi.org/10.1007/978-981-33-6785-2_1.

[11] R. Garcia-Fandino, Á. Piñeiro, Delving into the origin of destructive inflammation in COVID-19: a betrayal of natural host defense peptides? Front. Immunol. 11 (2021) 610024 https://doi.org/10.3389/fimmu.2020.610024.

[12] J. Pablo Palavicini, X. Han, Lipidomics of aging, in: Handb. Biol. Aging, Elsevier, 2021, pp. 391–404, https://doi.org/10.1016/B978-0-12-815962-0.00018-4.

[13] M. Saeedimasine, A. Montanino, S. Kleiven, A. Villa, Role of lipid composition on the structural and mechanical features of axonal membranes: a molecular simulation study, Sci. Rep. 9 (2019) 1–12, https://doi.org/10.1038/s41598-019-44318-9.

[14] D. Balleza, A. Alessandrini, M.J. Beltrán García, Role of lipid composition, physicochemical interactions, and membrane mechanics in the molecular actions of microbial cyclic lipopeptides, J. Membr. Biol. 252 (2019) 131–157, https://doi.org/10.1007/s00232-019-00067-4.

[15] D.R. Mittelstein, J. Ye, E.F. Schibber, A. Roychoudhury, L.T. Martinez, M. H. Fekrazad, M. Ortiz, P.P. Lee, M.G. Shapiro, M. Gharib, Selective ablation of cancer cells with low intensity pulsed ultrasound, Appl. Phys. Lett. 116 (2020) 013701, https://doi.org/10.1063/1.5128627.

[16] L.T. Nguyen, E.F. Haney, H.J. Vogel, The expanding scope of antimicrobial peptide structures and their modes of action, Trends Biotechnol. 29 (2011) 464–472, https://doi.org/10.1016/j.tibtech.2011.05.001.

[17] V.S. Bachu, J. Kedda, I. Suk, J.J. Green, B. Tyler, High-intensity focused ultrasound: a review of mechanisms and clinical applications, Ann. Biomed. Eng. 49 (2021) 1975–1991, https://doi.org/10.1007/s10439-021-02833-9.

[18] Z. Xu, T.L. Hall, E. Vlaisavljevich, F.T. Lee, Histotripsy: the first noninvasive, non-ionizing, non-thermal ablation technique based on ultrasound, Int. J. Hyperther. 38 (2021) 561–575, https://doi.org/10.1080/02656736.2021.1905189.

[19] V.H. Man, M.S. Li, J. Wang, P. Derreumaux, P.H. Nguyen, Interaction mechanism between the focused ultrasound and lipid membrane at the molecular level, J. Chem. Phys. 150 (2019) 215101, https://doi.org/10.1063/1.5099008.

[20] P. Tharkar, R. Varanasi, W.S.F. Wong, C.T. Jin, W. Chrzanowski, Nano-enhanced drug delivery and therapeutic ultrasound for cancer treatment and beyond, Front. Bioeng. Biotechnol. 7 (2019) 494402, https://doi.org/10.3389/fbioe.2019.00324.

[21] K. Entzian, A. Aigner, Drug delivery by ultrasound-responsive nanocarriers for cancer treatment, Pharmaceutics 13 (2021) 1135, https://doi.org/10.3390/pharmaceutics13081135.

[22] W.D. O'Brien, Ultrasound-biophysics mechanisms, Prog. Biophys. Mol. Biol. 93 (2007) 212–255, https://doi.org/10.1016/j.pbiomolbio.2006.07.010.

[23] V.H. Man, M.S. Li, P. Derreumaux, J. Wang, T.T. Nguyen, S. Nangia, P.H. Nguyen, Molecular mechanism of ultrasound interaction with a blood brain barrier model, J. Chem. Phys. 153 (2020) 045104, https://doi.org/10.1063/5.0010667.

[24] V.H. Man, M.S. Li, P. Derreumaux, J. Wang, P.H. Nguyen, Molecular mechanism of ultrasound-induced structural defects in liposomes: a nonequilibrium molecular dynamics simulation study, Langmuir 37 (2021) 7945–7954, https://doi.org/10.1021/acs.langmuir.1c00555.

[25] L.D. Johns, Nonthermal effects of therapeutic ultrasound: the frequency resonance hypothesis, J. Athl. Train. 37 (2002) 293–299. https://pmc.ncbi.nlm.nih.gov/articles/PMC164359/.

[26] N.H. Linh, V.H. Man, M.S. Li, J. Wang, P. Derreumaux, T.L. Mai, P.H. Nguyen, Molecular dynamics simulation of cancer cell membrane perforated by shockwave induced bubble collapse, J. Chem. Phys. 157 (2022) 225102, https://doi.org/10.1063/5.0105675.

[27] X.F. Wang, G. Tao, P. Wen, B.X. Ren, C.Q. Pang, C.X. Du, Damage to the DPPC membrane induced by shock waves: molecular dynamics simulations, J. Phys. Chem. B 124 (2020) 9535–9545, https://doi.org/10.1021/acs.jpcb.0c06077.

[28] R. Kfoury, B. Marzban, E. Makki, M.L. Greenfield, H. Yuan, Effect of pressure profile of shock waves on lipid membrane deformation, PLoS One 14 (2019) e0212566, https://doi.org/10.1371/journal.pone.0212566.

[29] M.O. Steinhauser, T. Schindler, Particle-based simulations of bilayer membranes: self-assembly, structural analysis, and shock-wave damage, Comput. Part. Mech. 4 (2017) 69–86, https://doi.org/10.1007/s40571-016-0126-3.

[30] Y. Sliozberg, T. Chantawansri, Damage in spherical cellular membrane generated by the shock waves: coarse-Grained molecular dynamics simulation of lipid vesicle, J. Chem. Phys. 141 (2014) 184904, https://doi.org/10.1063/1.4901130.

[31] D. Drikakis, J. Lechuga, S. Pal, Effects of shock waves on biological membranes: a molecular dynamics study, J. Comput. Theor. Nanosci. 6 (2009) 1437–1442, https://doi.org/10.1166/jctn.2009.1190.

[32] K. Koshiyama, T. Kodama, T. Yano, S. Fujikawa, Molecular dynamics simulation of structural changes of lipid bilayers induced by shock waves: effects of incident angles, Biochim. Biophys. Acta - Biomembr. 1778 (2008) 1423–1428, https://doi.org/10.1016/j.bbamem.2008.03.010.

[33] K. Koshiyama, T. Kodama, T. Yano, S. Fujikawa, Structural change in lipid bilayers and water penetration induced by shock waves: molecular dynamics simulations, Biophys. J. 91 (2006) 2198–2205, https://doi.org/10.1529/biophysj.105.077677.

[34] A. Blanco-González, S.J. Marrink, Á. Piñeiro, R. García-Fandiño, Molecular insights into the effects of focused ultrasound mechanotherapy on lipid bilayers: unlocking the keys to design effective treatments, J. Colloid Interface Sci. 650 (2023) 1201–1210, https://doi.org/10.1016/j.jcis.2023.07.077.

[35] H.J.C. Berendsen, J.P.M. Postma, W.F. Van Gunsteren, A. Dinola, J.R. Haak, Molecular dynamics with coupling to an external Bath, J. Chem. Phys. 81 (1984) 3684–3690, https://doi.org/10.1063/1.448118.

[36] S.J. Marrink, L. Monticelli, M.N. Melo, R. Alessandri, D.P. Tieleman, P.C.T. Souza, Two decades of martini: better beads, broader scope, Wiley Interdiscip. Rev. Comput. Mol. Sci. 13 (2023) e1620, https://doi.org/10.1002/wcms.1620.

[37] P.C.T. Souza, R. Alessandri, J. Barnoud, S. Thallmair, I. Faustino, F. Grünewald, I. Patmanidis, H. Abdizadeh, B.M.H. Bruininks, T.A. Wassenaar, P.C. Kroon, J. Melcr, V. Nieto, V. Corradi, H.M. Khan, J. Domański, M. Javanainen, H. Martinez-Seara, N. Reuter, R.B. Best, I. Vattulainen, L. Monticelli, X. Periole, D. P. Tieleman, A.H. de Vries, S.J. Marrink, Martini 3: a general purpose force field for coarse-grained molecular dynamics, Nat. Methods 18 (2021) 382–388, https://doi.org/10.1038/s41592-021-01098-3.

[38] P.C. Hsu, B.M.H. Bruininks, D. Jefferies, P. Cesar Telles de Souza, J. Lee, D.S. Patel, S.J. Marrink, Y. Qi, S. Khalid, W. Im, Charmm-gui martini maker for modeling and simulation of complex bacterial membranes with lipopolysaccharides, J. Comput. Chem. 38 (2017) 2354–2363, https://doi.org/10.1002/jcc.24895.

[39] Y. Qi, H.I. Ingólfsson, X. Cheng, J. Lee, S.J. Marrink, W. Im, CHARMM-GUI martini maker for coarse-grained simulations with the martini force field, J. Chem. Theory Comput. 11 (2015) 4486–4494, https://doi.org/10.1021/acs.jctc.5b00513.

[40] S. Jo, T. Kim, V.G. Iyer, W. Im, CHARMM-GUI: a web-based graphical user interface for CHARMM, J. Comput. Chem. 29 (2008) 1859–1865, https://doi.org/10.1002/jcc.20945.

[41] J. Lee, X. Cheng, J.M. Swails, M.S. Yeom, P.K. Eastman, J.A. Lemkul, S. Wei, J. Buckner, J.C. Jeong, Y. Qi, S. Jo, V.S. Pande, D.A. Case, C.L. Brooks, A. D. MacKerell, J.B. Klauda, W. Im, CHARMM-GUI input generator for NAMD, GROMACS, AMBER, OpenMM, and CHARMM/OpenMM simulations using the CHARMM36 additive force field, J. Chem. Theory Comput. 12 (2016) 405–413, https://doi.org/10.1021/acs.jctc.5b00935.

[42] H.B. Mann, D.R. Whitney, On a test of whether one of two random variables is stochastically larger than the other, Ann. Math. Stat. 18 (1947) 50–60, https://doi.org/10.1214/aoms/1177730491.

[43] Lindahl, Abraham, Hess, van der Spoel, GROMACS 2021.5 Manual, (n.d.). https://doi.org/10.5281/ZENODO.5849961.

[44] M.J. Abraham, T. Murtola, R. Schulz, S. Páll, J.C. Smith, B. Hess, E. Lindah, GROMACS: high performance molecular simulations through multi-level parallelism from laptops to supercomputers, SoftwareX 1–2 (2015) 19–25, https://doi.org/10.1016/J.SOFTX.2015.06.001.

[45] H.J.C. Berendsen, D. van der Spoel, R. van Drunen, GROMACS: a message-passing parallel molecular dynamics implementation, Comput. Phys. Commun. 91 (1995) 43–56, https://doi.org/10.1016/0010-4655(95)00042-E.

[46] C.R. Harris, K.J. Millman, S.J. van der Walt, R. Gommers, P. Virtanen, D. Cournapeau, E. Wieser, J. Taylor, S. Berg, N.J. Smith, R. Kern, M. Picus, S. Hoyer, M.H. van Kerkwijk, M. Brett, A. Haldane, J.F. del Río, M. Wiebe, P. Peterson, P. Gérard-Marchant, K. Sheppard, T. Reddy, W. Weckesser, H. Abbasi, C. Gohlke, T.E. Oliphant, Array programming with NumPy, Nature 585 (2020) 357–362, https://doi.org/10.1038/s41586-020-2649-2.

[47] R. Gowers, M. Linke, J. Barnoud, T. Reddy, M. Melo, S. Seyler, J. Domański, D. Dotson, S. Buchoux, I. Kenney, O. Beckstein, MDAnalysis: a python package for

the rapid analysis of molecular dynamics simulations, in: Proc. 15th Python Sci. Conf., Scipy, 2016, pp. 98–105, https://doi.org/10.25080/majora-629e541a-00e.
[48] N. Michaud-Agrawal, E.J. Denning, T.B. Woolf, O. Beckstein, MDAnalysis: a toolkit for the analysis of molecular dynamics simulations, J. Comput. Chem. 32 (2011) 2319–2327, https://doi.org/10.1002/jcc.21787.
[49] P. Virtanen, R. Gommers, T.E. Oliphant, M. Haberland, T. Reddy, D. Cournapeau, E. Burovski, P. Peterson, W. Weckesser, J. Bright, S.J. van der Walt, M. Brett, J. Wilson, K.J. Millman, N. Mayorov, A.R.J. Nelson, E. Jones, R. Kern, E. Larson, C. J. Carey, İ. Polat, Y. Feng, E.W. Moore, J. VanderPlas, D. Laxalde, J. Perktold, R. Cimrman, I. Henriksen, E.A. Quintero, C.R. Harris, A.M. Archibald, A.H. Ribeiro, F. Pedregosa, P. van Mulbregt, A. Vijaykumar, A. Pietro Bardelli, A. Rothberg, A. Hilboll, A. Kloeckner, A. Scopatz, A. Lee, A. Rokem, C.N. Woods, C. Fulton, C. Masson, C. Häggström, C. Fitzgerald, D.A. Nicholson, D.R. Hagen, D. V. Pasechnik, E. Olivetti, E. Martin, E. Wieser, F. Silva, F. Lenders, F. Wilhelm, G. Young, G.A. Price, G.L. Ingold, G.E. Allen, G.R. Lee, H. Audren, I. Probst, J. P. Dietrich, J. Silterra, J.T. Webber, J. Slavič, J. Nothman, J. Buchner, J. Kulick, J. L. Schönberger, J.V. de Miranda Cardoso, J. Reimer, J. Harrington, J.L. C. Rodríguez, J. Nunez-Iglesias, J. Kuczynski, K. Tritz, M. Thoma, M. Newville, M. Kümmerer, M. Bolingbroke, M. Tartre, M. Pak, N.J. Smith, N. Nowaczyk, N. Shebanov, O. Pavlyk, P.A. Brodtkorb, P. Lee, R.T. McGibbon, R. Feldbauer, S. Lewis, S. Tygier, S. Sievert, S. Vigna, S. Peterson, S. More, T. Pudlik, T. Oshima, T.J. Pingel, T.P. Robitaille, T. Spura, T.R. Jones, T. Cera, T. Leslie, T. Zito, T. Krauss, U. Upadhyay, Y.O. Halchenko, Y. Vázquez-Baeza, SciPy 1.0: fundamental algorithms for scientific computing in python, Nat. Methods 17 (2020) 261–272, https://doi.org/10.1038/s41592-019-0686-2.
[50] J.D. Hunter, Matplotlib: a 2D graphics environment, Comput. Sci. Eng. 9 (2007) 90–95, https://doi.org/10.1109/MCSE.2007.55.
[51] G. Bussi, D. Donadio, M. Parrinello, Canonical sampling through velocity rescaling, J. Chem. Phys. 126 (2007) 014101, https://doi.org/10.1063/1.2408420.
[52] H. Bhatia, H.I. Ingólfsson, T.S. Carpenter, F.C. Lightstone, P.T. Bremer, MemSurfer: a tool for robust computation and characterization of curved membranes, J. Chem. Theory Comput. 15 (2019) 6411–6421, https://doi.org/10.1021/acs.jctc.9b00453.
[53] M.F. Ergüder, M. Deserno, Identifying systematic errors in a power spectral analysis of simulated lipid membranes, J. Chem. Phys. 154 (2021) 214103, https://doi.org/10.1063/5.0049448.
[54] W. Humphrey, A. Dalke, K. Schulten, VMD: visual molecular dynamics, J. Mol. Graph. 14 (1996) 33–38, https://doi.org/10.1016/0263-7855(96)00018-5.
[55] Tomar, Converting video formats with FFmpeg, Linux J. Linux J 2006 (2022) 10. https://www.linuxjournal.com/article/8517. (Accessed 30 March 2025).
[56] J. Levy, D.L. Barrett, N. Harris, J.J. Jeong, X. Yang, S.C. Chen, High-frequency ultrasound in clinical dermatology: a review, Ultrasound J 13 (2021) 1–12, https://doi.org/10.1186/s13089-021-00222-w.
[57] A. Russo, A. Reginelli, G.V. Lacasella, E. Grassi, M.A.A. Karaboue, T. Quarto, G. M. Busetto, A. Aliprandi, R. Grassi, D. Berritto, Clinical application of ultra-high-frequency ultrasound, J. Personalized Med. 12 (2022) 1733, https://doi.org/10.3390/jpm12101733.
[58] D.L. Miller, N.B. Smith, M.R. Bailey, G.J. Czarnota, K. Hynynen, I.R.S. Makin, Overview of therapeutic ultrasound applications and safety considerations, J. Ultrasound Med. 31 (2012) 623–634, https://doi.org/10.7863/jum.2012.31.4.623.
[59] V.F. Humphrey, Ultrasound and matter-physical interactions, Prog. Biophys. Mol. Biol. 93 (2007) 195–211, https://doi.org/10.1016/j.pbiomolbio.2006.07.024.